

Isotopic insights into smoothening of abandoned fan surfaces, Southern California

Ari Matmon^{a,b,*}, Kyle Nichols^c, Robert Finkel^d

^a U.S. Geological Survey, 345 Middlefield Rd., MS #977, Menlo Park, CA 94025, USA

^b The Institute of Earth Sciences, Hebrew University, Givat Ram, Jerusalem, Israel 91904

^c Department of Geosciences, Skidmore College, 815 North Broadway, Saratoga Springs, NY 12866, USA

^d Lawrence Livermore National Laboratory, Livermore, CA 94550, USA

Received 26 May 2005

Available online 21 April 2006

Abstract

Cosmogenic nuclide concentrations measured on abandoned fan surfaces along the Mojave section of the San Andreas Fault suggest that sediment is generated, transported, and removed from the fans on the order of 30–40 kyr. We measured in situ produced cosmogenic ¹⁰Be, and in some cases ²⁶Al, in boulders ($n = 15$), surface sediment ($n = 15$), and one depth profile ($n = 9$). Nuclide concentrations in surface sediments and boulders underestimate fan ages, suggesting that ¹⁰Be accumulation is largely controlled by the geomorphic processes that operate on the surfaces of the fans and not by their ages.

Field observations, grain-size distribution, and cosmogenic nuclide data suggest that over time, boulders weather into grus and the bar sediments diffuse into the adjacent swales. As fans grow older the relief between bars and swales decreases, the sediment transport rate from bars to swales decreases, and the surface processes that erode the fan become uniform over the entire fan surface. The nuclide data therefore suggest that, over time, the difference in ¹⁰Be concentration between bars and swales increases to a maximum until the topographic relief between bars and swales is minimized, resulting in a common surface lowering rate and common ¹⁰Be concentrations across the fan. During this phase, the entire fan is lowered homogeneously at a rate of 10–15 mm kyr⁻¹.

© 2006 University of Washington. All rights reserved.

Keywords: ¹⁰Be; ²⁶Al; Nuclide concentration

Introduction

Quantifying rates of desert landscape change has challenged geomorphologists for more than a century due to slow rates of geomorphic processes over human time-scales (Gilbert, 1877; McGee, 1897). Traditional techniques, such as monitoring geomorphic change in deserts, require several years to decades to obtain useful information due to the limited rainfall (Abrahams et al., 1984; Schick and Lekach, 1993; Persico et al., 2005), yet, most monitoring studies do not capture the large, infrequent geomorphic events that have a major impact on the landscape (Kirchner et al., 2001). Some studies have relied on unique and rare geologic relations to quantify desert geomor-

phology (Oberlander, 1974), but such relations are not useful in most desert settings. Other dating techniques, especially radiocarbon dating, are not always applicable in harsh desert climates due to the lack of datable material.

For the past 20 years cosmogenic nuclides have become a common technique to date desert landforms (i.e. Klein et al., 1986; Bierman and Caffee, 2001). Cosmogenic nuclides minimize many of the problems described above: (1) cosmogenic nuclides average process rates over millennial time scales so they capture large and rare geomorphic events. (2) Unique geologic settings are not required as long as rocks with appropriate target minerals are present. (3) Cosmogenic nuclides can easily be measured in many different rock types, thus providing significant datable material.

Although the use of cosmogenic nuclides increases our understanding of desert geomorphology, there are still several assumptions that must be met. Some of the assumptions are

* Corresponding author. The Institute of Earth Sciences, Hebrew University, Givat Ram, Jerusalem, Israel 91904.

E-mail address: arimatmon@cc.huji.ac.il (A. Matmon).

difficult to address or constrain using field relations, such as nuclide inheritance from prior surface exposure, rock erosion, or complex geomorphic histories. For example, dating rocks on shorelines might yield ages that are too old for the shoreline due to unknown nuclide inheritance (Trull et al., 1995; Matmon et al., 2003). Other studies have shown that boulder or bedrock weathering causes underestimation of surface ages (Matmon et al., 2005). Nevertheless, cosmogenic nuclides have been used successfully to date desert pavements (Wells et al., 1995), date bedrock surface exposure age (Cockburn et al., 1999; Bierman and Caffee, 2001), and determine rates of tectonic deformation (Zehfuss et al., 2001; Matmon et al., 2005).

Similarly, cosmogenic nuclide concentrations in sediments have been used to quantify the rate of sediment deposition (Nichols et al., 2002), quantify the rate of sediment generation in arid basins (Granger et al., 1996; Clapp et al., 2000, 2001), quantify sediment budgets (Nichols et al., 2005), and trace sediment to determine long-term sediment transport rates (Nichols et al., 2002, 2005).

In this paper, we use cosmogenic ^{10}Be as an isotopic tracer in sediments on alluvial fans offset by the San Andreas Fault to determine how fan surfaces change over time. Thus, we are effectively substituting space (offset fans) for time (different durations of surface evolution). By using space-time substitution we show that surface processes, specifically boulder weathering, limit the time period of accurate cosmogenic nuclide exposure

ages. We also trace cosmogenic ^{10}Be from the boulders to the fan surface to quantify the evolution of young alluvial fan surfaces, dominated by irregular bar and swale topography, to smooth surfaces that characterize mature desert fans.

Geologic setting

The San Andreas Fault forms a 1100-km transform link between the Cape Mendocino triple junction and the Gulf of California seafloor-spreading zone and is part of the complex North American–Pacific plate boundary. The fault traverses most of coastal California; the Mojave section of the San Andreas Fault extends from the Cajon Creek in the southeast to Three Points in the northwest (Fig. 1). The climate along this section of the fault is mostly semi-arid with winter precipitation generated from cold fronts and summer precipitation generated from monsoon thunderstorms.

A series of alluvial fan remnants, numbered from 0 to 5, is aligned along the San Andreas Fault at distances ranging from 0.7 to 16.5 km from the present mouth of Little Rock Creek (LRC; Fig. 1, Barrows et al., 1985, Dibblee, 2002a,b). Fan ages increase with distance from the Little Rock Creek outlet (Matmon et al., 2005), and surface relief is inversely proportional to distance. The young fans have rough surfaces and bar-and-swale relief of as much as 10 m on their upper surface; the oldest fan has negligible surface relief. Natural

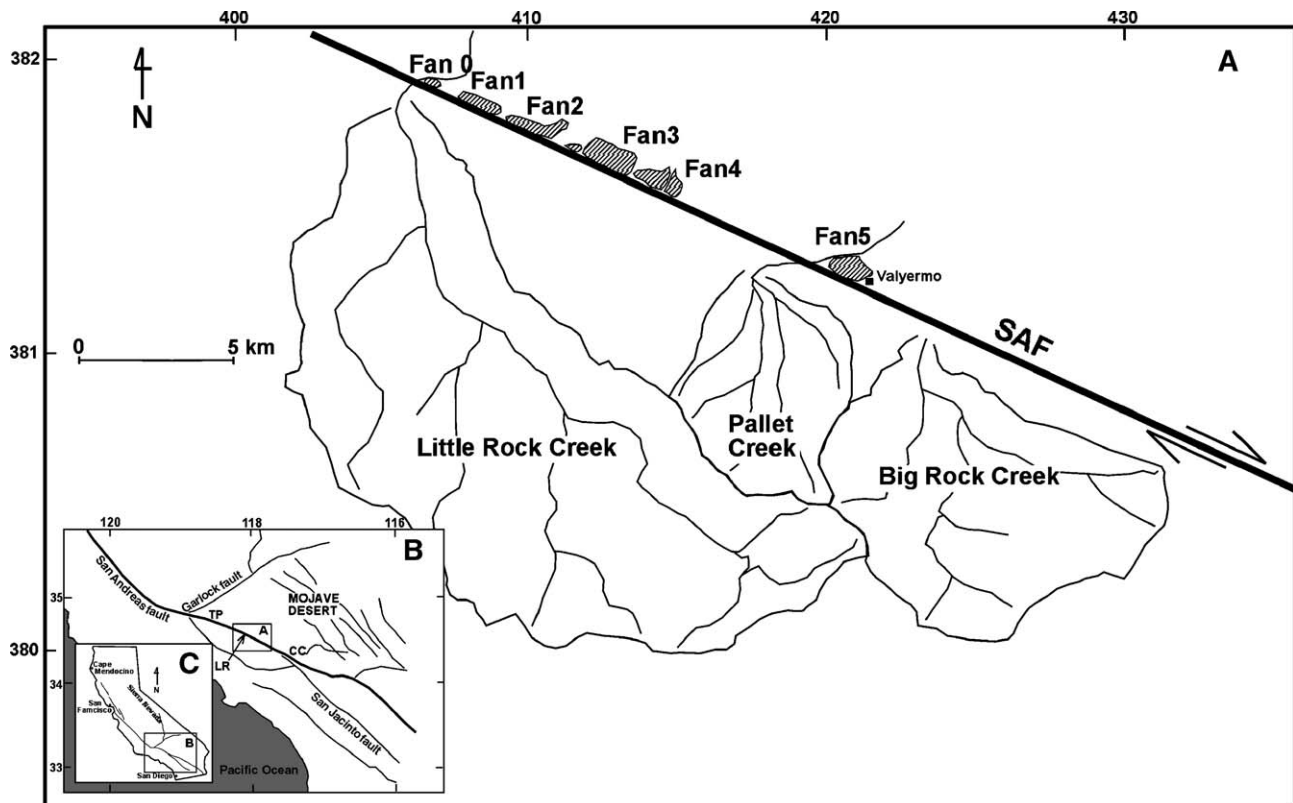


Figure 1. Geomorphic map and study location. (A) Little Rock Creek is the largest drainage system in the area with a drainage basin of approximately 200 km². SAF—San Andreas fault (thick line). Stripped areas indicate studied fans. Coordinates in UTM (Datum: NAD 27). (B and C) Maps showing location of study area (LR) and major faults in southern California. TP—Three Points, CC—Cajon Creek, Coordinates in Latitude Longitude.

streams and roads cut the fan deposits and expose deep cross sections with abundant boulders in all fans (Fig. 2A). However, the density of boulders exposed at the surface of

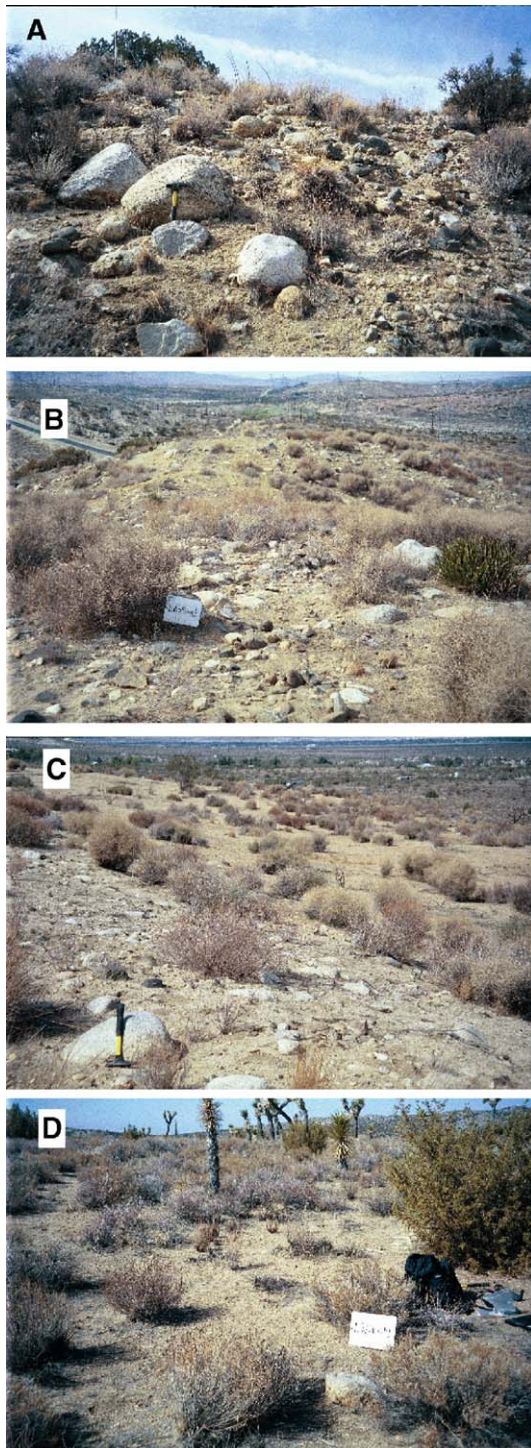


Figure 2. Photographs of fan surfaces. (A) Stream cut in fan 4 showing density of boulders in fan sediment at depth. Similar exposures in other studied fans indicate same density. (B) The upper surface of fan 1 is rough and contains many rounded and un-weathered boulders. Boulders are exposed on slopes of bars and in the swales as can be seen on far right. (C) Bar and swale on fan 4. Relatively few boulders are exposed on the bars. Boulders are not exposed on slopes between bars and swales nor in the swales (right side of the photo). (D) Upper surface of fan 5 is level and very few boulders are exposed.

the fans decreases with distance from the mouth of LRC. The decrease in boulder density at the surface is not uniform. Boulders are commonly exposed on bars and swales on the younger fans (0–1, Fig. 2B). On fans 2–4, boulders are mostly exposed on bars with few exposed boulders in the swales (Fig. 2C). On the farthest and oldest fan from LRC (fan 5), there are very few exposed boulders at the surface (Fig. 2D).

On the two youngest fans (0 and 1), exposed boulders are generally rounded and are not weathered. On progressively older fans (2 through 5), boulders are less rounded, occasionally cracked, slightly weathered, and sometimes coated with varnish. There is no systematic change in the degree of weathering of boulders among fans 2–5. The upper surfaces of the fans are not covered with desert pavement. The absence of desert pavement could be interpreted to suggest that the surface sediment is not stable over long time-scales. In contrast, the varnish-coated boulders suggest that boulders on the LRC fans reside at the surface longer than the surrounding sediment, long enough to allow a moderate degree of varnish to develop on them.

Methods

Based on the above field observations, we developed a hypothesis of the morphologic development of the fans' surfaces. Boulders are initially deposited uniformly on bars and in swales. Over time, the boulders weather into grus and the bar sediment is transported short distances into adjacent swales. As fans age, surface relief decreases, the sediment transport rate from bars to swales decreases, and the surface processes on the fan become uniform over the entire fan surface. At such time, the fan surface is lowered homogeneously. We designed our sampling protocol to test this hypothesis.

To determine the evolution of the alluvial fans we collected nine amalgamated sediment samples from bars and swales on the fan surfaces and seven amalgamated sediment samples from a depth profile on the oldest fan (fan 5). We also included data from fifteen boulders that were sampled for a previous study (Matmon et al., 2005; Table 1). The boulders from fans 0 and 1 are assumed to have been exposed since fan deposition and represent the age of the fan, when boulder erosion and inheritance are considered (Matmon et al., 2005). The ^{10}Be concentrations in boulders from fans 0 and 1 are not the result of erosional and transport processes that operated on the fans' surfaces after deposition and are not discussed in this study.

The sampled boulders generally stood at least 30 cm above their surrounding surface, except on fan 5 where surface boulders are small. All the boulders were rounded to sub-rounded and were either fresh or slightly weathered at the surface with no evidence of spalling. Sample thickness did not exceed 5 cm.

Seven amalgamated sediment samples were collected in a depth profile from a trench on the surface of fan 5 (Table 2, Fig. 3). The relatively smooth surface of fan 5 does not allow us to determine if the trench location represents a bar or a

Table 1
Cosmogenic ^{10}Be concentrations, model ages, and erosion rates for boulder samples from Little Rock Creek abandoned fan surfaces

| Name | Fan No. | Location (UTM NAD 27) | Elevation (m) | ^{10}Be (10^5 atoms g^{-1} quartz) | ^{26}Al (10^5 atoms g^{-1} quartz) | Normalized ^{10}Be (10^5 atoms g^{-1} quartz) | Normalized ^{26}Al (10^5 atoms g^{-1} quartz) | $^{26}\text{Al}/^{10}\text{Be}$ | Age (ka) | Erosion rate (mm kyr^{-1}) | Average fan erosion rate (mm kyr^{-1}) |
|---------|---------|-----------------------|---------------|---|---|--|--|---------------------------------|----------------|---------------------------------------|---|
| LROF-1 | 4 | 0413965/ 3815702 | 1088 | 3.80 ± 0.12 | | 2.03 ± 0.06 | | | 38.6 ± 4.1 | 25.4 ± 3.3 | 26.6 ± 3.5 |
| LROF-2 | 4 | 0414160/ 3815632 | 1089 | 3.50 ± 0.11 | 19.2 ± 1.54 | 1.74 ± 0.05 | 9.57 ± 0.77 | 5.50 ± 0.47 | 33.0 ± 3.5 | 27.7 ± 3.6 | |
| LROF-3 | 4 | 0414408/ 3815409 | 1094 | 3.63 ± 0.12 | | 1.95 ± 0.06 | | | 25.4 ± 2.8 | 26.6 ± 3.5 | |
| LROF-6 | 3 | 0412785/ 3816208 | 1096 | 2.40 ± 0.29 | | 1.28 ± 0.15 | | | 24.3 ± 3.8 | 41.2 ± 5.4 | 28.7 ± 3.9 |
| LROF-7 | 3 | 0412693/ 3816342 | 1090 | 5.29 ± 0.17 | 31.7 ± 2.17 | 2.83 ± 0.08 | 17.0 ± 1.16 | 6.00 ± 0.45 | 54.0 ± 5.7 | 17.9 ± 2.3 | |
| LROF-8 | 3 | 0412541/ 3816379 | 1089 | 4.00 ± 0.13 | 23.1 ± 1.12 | 2.00 ± 0.06 | 11.6 ± 0.56 | 5.80 ± 0.67 | 40.6 ± 4.3 | 24.1 ± 3.1 | |
| LROF-9 | 3 | 0412306/ 3816548 | 1089 | 3.08 ± 0.11 | | 1.65 ± 0.06 | | | 31.3 ± 3.4 | 31.6 ± 4.1 | |
| LROF-10 | 3 | 0412361/ 3816411 | 1078 | 7.53 ± 0.26 | | 4.04 ± 0.14 | | | 77.3 ± 8.3 | 12.0 ± 1.6 | |
| LROF-11 | 2 | 0410747/ 3817155 | 1028 | 3.28 ± 0.10 | | 1.76 ± 0.06 | | | 33.3 ± 3.5 | 28.4 ± 3.7 | 29.3 ± 4.1 |
| LROF-12 | 2 | 0410262/ 3817394 | 1043 | 1.98 ± 0.08 | 11.9 ± 0.65 | 1.03 ± 0.04 | 6.36 ± 0.35 | 5.99 ± 0.40 | 20.1 ± 2.2 | 48.4 ± 6.3 | |
| LROF-13 | 2 | 0410002/ 3817529 | 1050 | 3.91 ± 0.14 | | 2.09 ± 0.07 | | | 39.8 ± 4.3 | 23.9 ± 3.1 | |
| LROF-14 | 2 | 0410940/ 3817469 | 1032 | 5.46 ± 0.17 | 30.9 ± 2.10 | 2.93 ± 0.09 | 16.5 ± 1.12 | 5.65 ± 0.42 | 55.8 ± 5.9 | 16.5 ± 2.1 | |
| LROF-19 | 5 | 0420382/ 3812510 | 1178 | 8.50 ± 0.26 | | 4.00 ± 0.12 | | | 76.5 ± 8.2 | 11.3 ± 1.5 | 11.0 ± 1.4 |
| LROF-20 | 5 | 0420472/ 3812625 | 1181 | 8.78 ± 0.33 | | 4.11 ± 0.15 | | | 78.9 ± 8.6 | 11.0 ± 1.4 | |
| LROF-21 | 5 | 0420700/ 3812567 | 1178 | 8.94 ± 0.28 | 57.1 ± 2.65 | 4.20 ± 0.13 | 26.8 ± 1.24 | 6.31 ± 0.63 | 80.6 ± 8.6 | 10.7 ± 1.4 | |

Measured concentrations were normalized using scaling factors from Lal (1991) for nucleonic production and Granger and Smith (2000) for muogenic production. Ages and erosion rates calculated using a high latitude, sea level total production rate of $5.37 \text{ }^{10}\text{Be}$ atoms g^{-1} quartz (Schaller et al., 2001) of which 2.6% are caused by muons (Granger and Smith, 2000). Erosion rate calculations follow Granger and Muzikar (2001). Production rates were not corrected for boulder geometry (Masarik and Wieler, 2003) and for variation in the paleomagnetic field (Pigati and Lifton, 2004). Concentration measurements include analytical errors and AMS counting errors. Ages and erosion rates include analytical errors and a propagated 10% uncertainty in production rate.

swale. Samples were collected at 20-cm intervals from depths of 30 to 170 cm. The upper 30 cm showed abundant evidence of bioturbation and were not sampled. All the samples were sieved and the 0.25–0.85 mm grain size fraction was processed and analyzed for ^{10}Be concentration. The >10 mm fraction was also analyzed in the uppermost (LRDP-1 [30–50]) and lowermost (LRDP-1 [150–170]) profile samples.

Nine sediment samples were collected from the surfaces of the fans (Table 2). Two samples, one from the bars and one from the swales, were collected from each fan. Samples were not collected from fan 2 due to surface disturbance by human activity. Fan 0 is currently being incised by LRC and its area has been significantly reduced. Furthermore, human activity left few undisturbed surfaces. Therefore, only an amalgamated bar sample was collected from fan 0. Samples were collected by amalgamating the top centimeter of grus from several bars or swales on each fan. Each sample, therefore, includes sediment from across the bars or the swales and the measured ^{10}Be concentrations represent an average of the sampled area. All the

samples were sieved and separated into four grain sizes (0.25–0.85 mm, 0.85–2.8 mm, 2.8–11.2 mm, >11.2 mm) and each fraction was weighed to determine relative abundance (Fig. 4). To determine whether differential sediment transport from bars to swales controls the ^{10}Be concentrations from the first stages of fan surface development, and if bar material erodes homogeneously during the last stages of fan surface development, all four grain size fractions were analyzed for ^{10}Be in the sample collected from the swales on fan 1 (FN1SD2) and the sample collected from the bars on fan 4 (FN4SD1). In all the other samples, only the 0.25–0.85 mm fraction was analyzed. All samples were processed following procedures in Bierman and Caffee (2001) and isotopic ratios were measured at the Lawrence Livermore National Laboratory. To translate the nuclide concentrations measured in boulder samples into surface exposure ages and rates of change, we accounted for production by secondary neutrons and muons and used model parameters established previously (Table 1). For sediment samples, we also accounted for production by secondary neutrons and muons. Using a Monte Carlo approach, we calculated the median and

Table 2
Cosmogenic ¹⁰Be concentrations of surface and buried sediment samples from Little Rock Creek abandoned fan surfaces

| Name | Fan no. | Elevation (m) | ¹⁰ Be (10 ⁵ atoms g ⁻¹ quartz) | Normalized ¹⁰ Be (10 ⁵ atoms g ⁻¹ quartz) |
|------------------------------|---------|---------------|---|--|
| FN0SD1 (0.25–0.85) | 0 | 943 | 1.49 ± 0.08 | 0.65 ± 0.03 |
| FN1SD1 (0.25–0.85) | 1 | 977 | 2.81 ± 0.09 | 1.17 ± 0.04 |
| FN1SD2 (0.25–0.85) | 1 | 967 | 2.55 ± 0.08 | 1.07 ± 0.04 |
| FN1SD2 (0.85–2.8) | 1 | 967 | 3.13 ± 0.11 | 1.31 ± 0.05 |
| FN1SD2 (2.8–11.2) | 1 | 967 | 3.12 ± 0.10 | 1.31 ± 0.04 |
| FN1SD2 (>11.2) | 1 | 967 | 3.63 ± 0.12 | 1.52 ± 0.05 |
| FN3SD1 (0.25–0.85) | 3 | 1090 | 2.24 ± 0.12 | 0.86 ± 0.05 |
| FN3SD2 (0.25–0.85) | 3 | 1076 | 5.26 ± 0.17 | 2.02 ± 0.06 |
| FN4SD1 (0.25–0.85) | 4 | 1090 | 2.31 ± 0.08 | 0.88 ± 0.03 |
| FN4SD1 (0.85–2.8) | 4 | 1090 | 2.39 ± 0.08 | 0.91 ± 0.03 |
| FN4SD1 (2.8–11.2) | 4 | 1090 | 2.26 ± 0.08 | 0.86 ± 0.03 |
| FN4SD1 (>11.2) | 4 | 1090 | 2.46 ± 0.08 | 0.94 ± 0.03 |
| FN4SD2 (0.25–0.85) | 4 | 1086 | 3.86 ± 0.13 | 1.47 ± 0.05 |
| FN5SD1 (0.25–0.85) | 5 | 1182 | 5.25 ± 0.14 | 1.86 ± 0.05 |
| FN5SD2 (0.25–0.85) | 5 | 1182 | 5.62 ± 0.22 | 1.98 ± 0.06 |
| <i>Depth profile (fan 5)</i> | | | | |
| LRDP-1 (150–170) | 5 | 1180 | 0.92 ± 0.04 | |
| LRDP-1 (150–170) >10 | 5 | 1180 | 0.78 ± 0.04 | |
| LRDP-1 (130–150) | 5 | 1180 | 1.44 ± 0.05 | |
| LRDP-1 (110–130) | 5 | 1180 | 1.71 ± 0.06 | |
| LRDP-1 (90–110) | 5 | 1180 | 2.09 ± 0.07 | |
| LRDP-1 (70–90) | 5 | 1180 | 2.60 ± 0.09 | |
| LRDP-1 (50–70) | 5 | 1180 | 3.49 ± 0.15 | |
| LRDP-1 (30–50) | 5 | 1180 | 4.67 ± 0.15 | |
| LRDP-1 (30–50) >10 | 5 | 1180 | 4.41 ± 0.26 | |

Measured concentrations were normalized using scaling factors from Lal (1991) for nucleonic production and Granger and Smith (2000) for muogenic production.

Concentration measurements include analytical errors and AMS counting errors.

most likely apparent age of each sediment sample (Fig. 5) in order to estimate the residence time of sediment on the fans. Ages were calculated following equations in Brown et al. (1998). The inherited values were taken from measured ¹⁰Be concentrations in sand-size sediment collected from the LRC active channel (Matmon et al., 2005).

Results

Boulders

Boulder samples exhibit a large range in ¹⁰Be concentrations. Nuclide concentrations in boulders sampled from fans 2–5 range between 8.9 ± 0.3 × 10⁵ and 2.9 ± 0.1 × 10⁵ atoms g⁻¹ quartz (Table 1). Boulders from fans 2 and 3 have a large range of ¹⁰Be concentrations while boulders from fans 4 and 5 have a small range. The average ¹⁰Be concentration on fan 2 is similar to that on fan 3 (excluding sample LROF-10; see explanation below) and fan 4 at ~3.7 ± 0.15 × 10⁵ atoms g⁻¹ quartz. Concentrations of ²⁶Al, analyzed in 6 boulders range between 11.9 ± 0.7 × 10⁵ and 57.1 ± 2.7 × 10⁵ atoms g⁻¹ quartz (Table 1). ²⁶Al /¹⁰Be ratios range between 5.5 ± 0.5 and 6.3 ± 0.6 (Table 1).

We use the boulders to determine the average fan surface lowering rates for fans 2 through 5. Four boulders were sampled from the surface of fan 2 (Table 1, Fig. 5). The average model lowering rate of fan 2, calculated from ¹⁰Be concentrations in the boulders collected from bars is 29.3 ± 4.1 mm kyr⁻¹. On fan 3, four boulders collected from bars yielded a ¹⁰Be average lowering rate of 28.7 ± 3.9 mm kyr⁻¹. One boulder collected from a swale yielded a model lowering rate of 12.0 ± 1.6 mm kyr⁻¹. On fan 4, we could not locate, nor sample, boulders from the swales. Three boulders from bars suggest an average lowering rate of 26.6 ± 3.5 mm kyr⁻¹ (Table 1), similar to lowering rate of the boulders sampled from the bars of fan 2 and fan 3. On fan 5, there are very few boulders at the surface. We sampled three small boulders that yielded ¹⁰Be concentrations that correspond to an average lowering rate of 11.0 ± 1.4 mm kyr⁻¹.

Depth profile samples

The ¹⁰Be concentrations in the depth profile samples on fan 5 decrease exponentially from 4.67 ± 0.15 × 10⁵ atoms of ¹⁰Be g⁻¹ quartz (near the surface) to 0.92 ± 0.04 × 10⁵ atoms of ¹⁰Be g⁻¹ quartz at depth (Fig. 3, Table 2). ¹⁰Be concentrations in fine

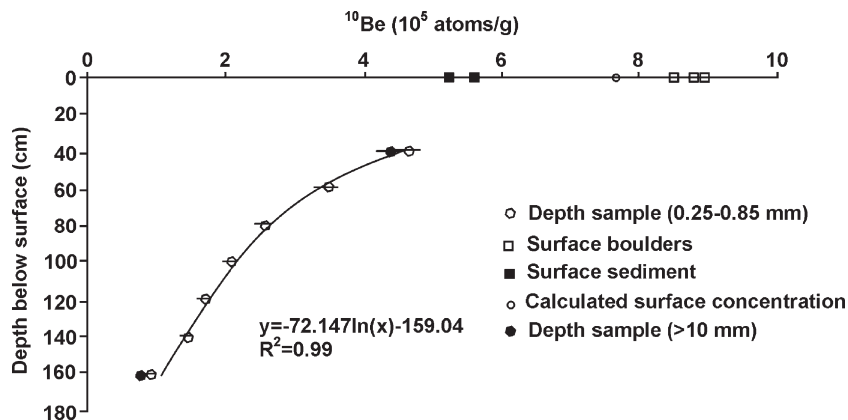


Figure 3. Depth profile in fan 5. ¹⁰Be concentrations of boulder samples LROF-19, LROF-20, and LROF-21 are indicated as surface boulders. ¹⁰Be concentrations of samples FN5SD1 and FN5SD2 are indicated as surface sediment. Model surface concentration was calculated by extrapolating the depth samples exponential fit to the surface.

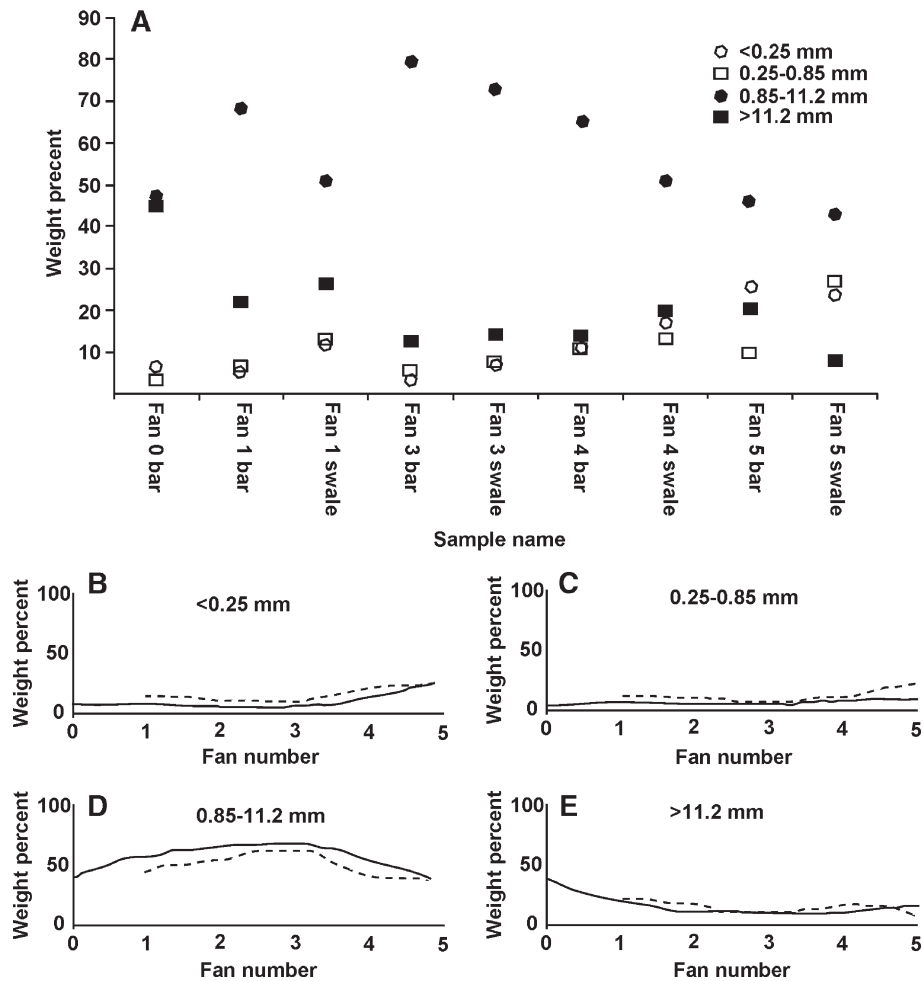


Figure 4. Grain size distribution in the sediment samples. The 0.85- to 11.2-mm fraction is the most abundant in all the sediment samples (A). Each grain fraction has a distinctive trend over the range of fans (B–E). Fractions of grain size in bars indicated by black solid lines and in swales by dashed lines. On each fan, the 0.25–0.85 mm fraction is higher in swales than on bars (C) and the 0.85–11.2 mm fraction is higher on bars than in swales (D). The <0.25-mm fraction is relatively low in all the samples (A) but increases with fan age (B). On fans with distinct bars and swales, the <0.25-mm fraction is higher in swales than on bars. On fan 5, where relief is insignificant, the <0.25-mm fraction is similar across the fan surface.

(0.25–0.85 mm), and coarse (>10 mm) grain size fractions were similar in both the lowermost (LRDP-1 [150–170]) and uppermost samples (LRDP-1 [30–50] (Table 2).

Sediment

The grain-size distribution on each fan shows several distinctive characteristics (Fig. 4). The most abundant grain size in all the sediment samples probably represents the normal range of crystal sizes in the granitic boulders on the fans (0.85 to 11.2 mm, Fig. 4A) suggesting that the grain size distribution is controlled by the crystal sizes in the bedrock. The abundance of this grain size through time suggests that after boulder disintegration, the individual grains erode slowly.

Each grain fraction has a distinctive trend over the range of fans. The weight percentage of the 0.85–11.2 mm fraction in swales increases from 46% on fan 0 to a maximum of 79% on fan 3 and then decreases to 43% on fan 5 (Fig. 4D). On each fan, the percentages of the 0.25–0.85 mm and <0.25-mm fractions are slightly higher in the swales than on the bars and the 0.85–

11.2 mm fraction is higher on the bars than in the swales (Figs. 4C and D), suggesting that small grains move from bars to swales faster than large grains or that larger grains break into smaller ones during residence in the swales. Overall, the <0.25-mm fraction, which could originate from eolian input and/or from weathering of micas and feldspars, is relatively low in all the samples but increases from 6% on fan 0 to ~24% on fan 5 (Fig. 4B). On all the fans that have distinctive bars and swales, the <0.25-mm fraction is higher in the swales than on the bars, probably a result of the faster transport of fine size particles into the swales. On fan 5, where relief is insignificant, the <0.25-mm fraction is similar across the fan surface.

The concentrations of ^{10}Be in the surface sediment samples range between $1.5 \pm 0.1 \times 10^5$ and $5.3 \pm 0.2 \times 10^5$ atoms g^{-1} quartz (Table 2). On all the fans, bar sediment yields an equal or lower ^{10}Be concentration than swale sediment (Fig. 5, Table 1). The grain size fractions of two sediment samples have different ^{10}Be trends. The ^{10}Be data of swale sediment collected from fan 1 (FN1SD2) range between $2.55 \pm 0.08 \times 10^5$ (0.25–0.85 mm) and $3.63 \pm 0.12 \times 10^5$ atoms g^{-1} quartz (>11.2 mm, Fig. 5A,

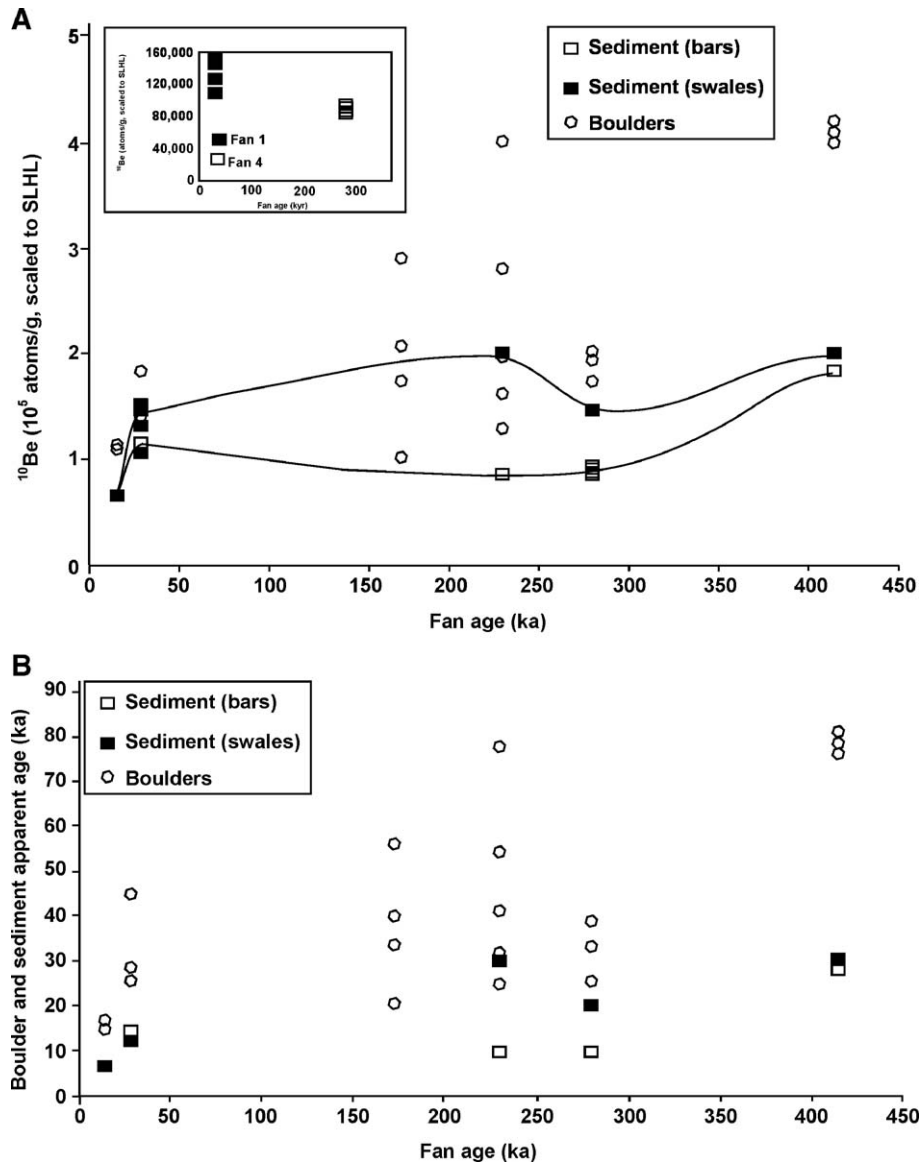


Figure 5. A. ^{10}Be concentrations, scaled to sea level and high latitude (SLHL) in sediments and boulders from bars and swales on the LRC fans. Fan ages are taken from Matmon et al. (2005). The age of fan 2 was calculated from its offset from LRC and the slip rates calculated in Matmon et al. (2005). On all fans, the nuclide concentrations in boulders are higher than in sediments. This is due to longer residence time of boulders on the fan surfaces and bioturbation of sediment which mixes dosed surface sediment with less dosed sediment from the subsurface. Inset graph shows ^{10}Be concentrations (atoms g^{-1} quartz) of four grain sizes for fan 1 swale sediment and fan 4 bar sediment. In the swales, larger grain sizes have higher ^{10}Be . On the bars, all grain sizes have similar ^{10}Be concentrations. B. Sediment and boulder apparent ages as a function of fan age. Fan 1 swale age and fan 4 bar age are averages of ages calculated from all grain sizes. See text for further explanation. Error bars (see Tables 1 and 2) were removed for clarity.

Table 2). The average ^{10}Be concentration of all grain size fractions is $3.11 \pm 0.10 \times 10^5$ atoms g^{-1} , higher than the ^{10}Be concentration of the sample collected from the bar on fan 1 ($2.81 \pm 0.09 \times 10^5$ atoms g^{-1}). In the sample collected from the bars of fan 4 (FN4SD1), ^{10}Be concentrations of the different grain sizes are fairly uniform and only range between $2.26 \pm 0.08 \times 10^5$ (2.8 to 11.2 mm) and $2.46 \pm 0.08 \times 10^5$ atoms of ^{10}Be g^{-1} quartz (>11.2 mm).

Discussion

The nuclide concentrations of the surface boulders, the depth profile, and the surface sediment are controlled by the rate of

weathering and sediment removal from the fan surfaces. Nuclide concentrations in boulders reveal how quickly the fan surfaces are eroding. The depth profile allows us to estimate fan 5’s surface lowering rate. Nuclide concentrations in surface sediment reflect the rate that surface processes reshape fan surfaces. Together, these samples provide a timeframe for the surface evolution of the granitic fan surfaces in this part of the western Mojave Desert.

Insights from boulders

Exposure age dating of the investigated fan surfaces showed that surface boulder samples do not always represent the fan’s

age (Matmon et al., 2005). On the young fans (0–1), fan surface lowering is not significant and cosmogenic nuclides in boulders do represent the surface age (16 ± 5 ka and 29 ± 7 ka) when boulder erosion and inheritance are taken into account. Boulders from fan 2, 3 and 4 exhibit a similar range of exposure ages: 20.1 ± 2.2 to 55.8 ± 5.9 ka (fan 2), 24.3 ± 3.8 to 77.3 ± 8.3 ka (fan 3), and 25.4 ± 2.8 to 38.6 ± 4.1 ka (fan 4) (Matmon et al., 2005). Yet, the fan ages are estimated at ~ 170 ka for fan 2, based on its offset from the mouth of LRC and the slip rate along the San Andreas fault, 220 ± 240 ka for fan 3, and 280 ± 185 ka for fan 4 based on $^{26}\text{Al}/^{10}\text{Be}$ ratios of deeply buried sediment (Matmon et al., 2005). Fan 5 has boulder exposure ages that range between 76.5 ± 8.2 and 92.2 ± 9.9 ka, and a buried sediment $^{26}\text{Al}/^{10}\text{Be}$ age of 413 ± 180 ka (Matmon et al., 2005). Based on the significant disparities between boulder apparent exposure ages and fan ages we conclude that the ^{10}Be concentrations in the boulders sampled from the surfaces of fans 2–5, which have an $^{26}\text{Al}/^{10}\text{Be}$ ratio of ~ 6 (Table 1), are controlled by the rate of lowering of the fans' surfaces and thus the rate of boulder exposure.

The similar ^{10}Be concentrations in boulders collected from bars on fans 2, 3, and 4, and the resulting model erosion rates, suggest that these fan surfaces are eroding at a similar average rate of 28.2 ± 3.8 mm kyr $^{-1}$. Such uniform erosion rates indicate that a balance between sediment generation and sediment removal on the bars was achieved by ~ 170 ka (the age of fan 2) or less. However, these data can be interpreted in an alternative and, in our opinion, more convincing way. On any fan, some boulders could have been, and probably were, exposed many thousands of years before other boulders. Thus, the boulders with high ^{10}Be concentrations represent the accumulation of nuclides during exhumation and long surface exposure, while boulders with low ^{10}Be concentrations represent exhumation and shorter exposure periods. This explanation is supported by the large range of ^{10}Be concentration in boulders on each fan. Using the lowest dosed boulder on each fan to model fan surface erosion rates, we determine that fan surface lowering rates decrease as fan ages increase: 48 ± 6 mm kyr $^{-1}$ for fan 2, 41 ± 5 mm kyr $^{-1}$ for fan 3, 28 ± 4 mm kyr $^{-1}$ for fan 4, and 11 ± 2 mm kyr $^{-1}$ for fan 5. In spite of the small number of boulders analyzed from each fan, the results are consistent with the decreasing topographic relief of the fan surfaces over time.

The average surface lowering rate of fan 5, based on the boulders (11.0 ± 1.4 mm kyr $^{-1}$), is less than the surface lowering rates of fans 2–5 based on bar boulders, but similar to surface lowering rate of fan 3 based on the swale boulder (LROF-10, 12.0 ± 1.6 mm kyr $^{-1}$). This similarity might suggest that the lowering rate of the swales has stabilized by ~ 220 ka (the age of fan 3).

Depth profile

A depth profile from the surface of fan 5 shows an exponential decrease in ^{10}Be concentrations with increasing depth (Fig. 3, Table 2). The exceptional model fit of the data suggests that there have not been major events of stripping or deposition of material that altered the fan's surface and its

continuous erosion. By projecting the profile to the surface we can estimate the surface lowering rate.

At the surface of fan 5, the model fit yields a ^{10}Be concentration of 7.6×10^5 atoms g $^{-1}$ quartz, consistent with a surface lowering rate of 12.7 ± 1.7 mm kyr $^{-1}$ (Fig. 3). The lowering rate based on the depth profile is intermediate between the estimate indicated by the boulders (11.0 ± 1.4 mm kyr $^{-1}$) and the estimate indicated by the surface sediments of fan 5 (15 – 18 mm kyr $^{-1}$). Such differences are caused by the processes that operate at the surface of fan 5. The model-fit ^{10}Be concentration does not consider bioturbation and assumes that all material is removed from the surface at the same rate it is generated, i.e., steady-state erosion. However, bioturbation does occur and surface material is mixed with material from as deep as 30–40 cm. Thus, the average ^{10}Be concentration of surface sediment is lower than the modeled concentration, suggesting higher rates of surface erosion than actually occurs. On the other hand, the few boulders that reach the surface are more stable than the surface sediment. Thus, their exposure time is longer, their ^{10}Be concentrations are higher, and the modeled surface erosion rates are slower. Different grain size fractions in each of the two samples in the depth profile (LRDP-1 [150–170] and LRDP-1 [30–50]) have similar nuclide concentrations (Table 2). Such consistent nuclide concentrations suggest that all grain sizes are generated and exhumed to the surface at similar rates.

Surface sediments

The nuclide concentrations of surface sediments provide insight into the difference between bar and swale processes, the behavior of different grain sizes, and the residence time of sediment on fan surfaces during transport. On active fans, nuclide concentrations of bar sediment and swale sediment are similar because the time required to allow surface processes to alter ^{10}Be concentrations is short (Table 2). As the fans mature, bar sediment is transported to the swales causing swale sediment to be more highly dosed than the newly exposed bar sediment (Fig. 5). Sediment transport and the nuclide disparity between highly dosed swale sediment and lower dosed bar sediment continues until the topographic difference between bars and swales decrease enough to allow surface processes to reach steady state. On the LRC fans, the differences in nuclide concentrations reach a maximum at about 220 ka on fan 3 (Fig. 5). It is possible that this maximum has already been reached on fan 2, ~ 170 kyr since deposition, but we cannot distinguish between bars and swales on this fan due to surface disturbance caused by human activity. As fan surface relief decreases, the nuclide activity of swale sediment approaches a steady state value representative of overall surface lowering (Table 2, Fig. 5). The ^{10}Be concentration of sediments collected from the swales in fan 4, however, is an exception. It is lower than the ^{10}Be concentrations of sediments from swales collected from fans 3 and 5. The low nuclide concentration of fan 4 swale sediments might have resulted from an erosional event that exposed less dosed material. Nuclide concentrations measured in a swale boulder from fan 3 and from the surface boulders of fan 5 are similar, but are higher than the nuclide concentrations

measured in the swale sediments from these fans. The difference in steady-state ^{10}Be concentrations between sediment and boulders probably reflects the fact that fine-grained swale sediment is transported more rapidly off the fan surfaces than boulders.

Nuclide concentrations in different grain sizes reveal the tempo of bar and swale processes. In the sample collected from a bar on fan 4 (FN4SD1), there is no difference in ^{10}Be concentrations between the different grain sizes. The similarity in nuclide concentrations suggests that boulder erosion supplies a range of grain sizes at similar rates. This result is also supported by similar ^{10}Be concentrations in the different grain sizes measured in two depth profile samples (Table 2). However, in the swales on fan 1, the smaller grain sizes have lower ^{10}Be concentrations than the larger grains. Thus, the disparity in the concentrations of ^{10}Be in grain sizes occurs during transport from bars to swales; smaller grains are transported faster from bars to swales than the larger grains. The preferential transport of small grain sizes is supported by a higher percentage of smaller grain sizes in the swales (Fig. 4). We can use the ^{10}Be grain size data from the swale in fan 1 to determine the difference in residence time of different grain sizes. The ^{10}Be nuclide difference between the small grains and the large grains is 1.07×10^5 atoms g^{-1} , which is equivalent to 8.5 kyr of surface exposure. Thus, the coarse grains reside on the fan surface several millennia longer, on average, than fine grains.

The nuclide concentration of surface sediment is controlled by the rate of surface change. The sediment reaches nuclide steady state as a function of fan surface lowering rate, boulder erosion rate, transport rate of sediment from bars to swales, and nuclide decay. The steady state ^{10}Be concentration in the sediment represents the average time that sediment spends on the fan from first exposure to cosmic rays, as the fan surface is being lowered, until it is removed from the fan entirely. Nuclide concentrations in swale sediment from fan 3 and from fan 5 range between $5.3 \pm 0.13 \times 10^5$ and $5.6 \pm 0.2 \times 10^5$ atoms of ^{10}Be g^{-1} quartz. These concentrations correspond to an exposure time that ranges between 35.2 ± 3.7 and 38.4 ± 4.1 kyr. When an inherited dose is considered, given by the average ^{10}Be concentration of 0.55×10^5 atoms of ^{10}Be g^{-1} quartz in fine sandy sediments in the active channel of Little Rock Creek (Matmon et al., 2005), the ^{10}Be concentrations in sediment collected from the swale of fan 3 and from the surface of fan 5 correlate to ages that range between 30.4 ± 3.2 and 32.8 ± 3.5 ka. Thus, it appears that generation of sediment and its transport through the swales and off the LRC fans takes on the order of 30 kyr or more.

Conclusions

We integrate field observations, grain size distribution, and cosmogenic nuclide data to derive the following description of the morphologic development of fan surfaces in the study area. At the time of deposition, all grain sizes from sand to boulders are deposited on bars and swales with a common nuclide inheritance (Fig. 6A). As fan surfaces age, boulders weather

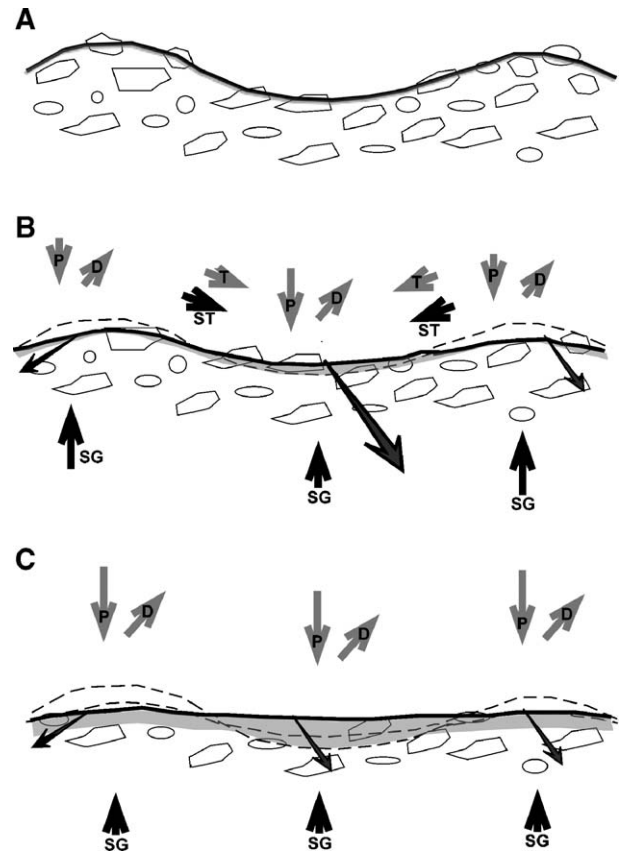


Figure 6. Cartoon showing the mass balance and cosmogenic nuclide balance on abandoned fan surfaces in the LRC area. Black arrows indicate mass. Gray arrows indicate ^{10}Be . P—Production of ^{10}Be at the surface. D—Decay of ^{10}Be . T—Transport of ^{10}Be from bars to swales. ST—Sediment transport from bars to swales. SG—Sediment generation from boulder erosion and fan surface lowering. Diagonal black arrows with gray centers indicate removal of mass and ^{10}Be off the fan. Length of transport arrow indicates relative flux. (A) Initial condition. Boulders are randomly scattered in the fan. (B) Intermediate condition. Bars are lowered by weathering of boulders and transport of material to swales. Lowering of swales is partially compensated by accumulation of material transported from bars (gray areas). Dashed lines represent pre-lowering surface. ^{10}Be accumulates faster in the swales. On average, the entire fan is being lowered. (C) Final condition. Fan surface is topographically uniform. Lowering rate and ^{10}Be accumulation rates are similar throughout the fan.

into grus, the relief between bars and swales decreases, the sediment transport rate from bars to swales decreases, and the surface processes that modify the fan became approximately uniform over the entire fan surface (Figs. 6B and C). At such time, the entire fan is lowered homogeneously.

Surface processes not only move sediment, they also control the concentrations of ^{10}Be in the geomorphic units. The ^{10}Be concentration in bar sediment is a balance between nuclide production (production in the target sedimentary material, the addition from substrate during surface lowering, and the rate at which boulders are eroding to grus) and nuclide removal (nuclide decay and the transport of sediment from the bars to the swales; Fig. 6). Similarly, the ^{10}Be concentration in swale sediment is balanced between production (in the target sedimentary material and the supply from sediment delivered from the bars) and removal (decay and transport of sediment off the fan). The difference in ^{10}Be concentration between bar

sediment and swale sediment increases to a maximum (fan 3) until such time that the topographic relief between bars and swales is minimized, resulting in a common surface lowering rate and common ^{10}Be concentrations across the fan (Figs. 5 and 6).

On LRC fan surfaces, cosmogenic nuclide data suggest that sediment is generated, transported, and removed from the fans over time periods of 30–40 kyr. The residence time of bar sediment is shorter than swale sediment; fine-grain sediment is removed from bars faster than coarse-grained sediment. Nuclide concentrations of swale sediment might reach steady state by 220 kyr, or perhaps as early as 170 kyr, after deposition of the fan. Bar and swale topography are reduced to a relatively smooth surface and erosion processes become homogeneous across fan surfaces by 280–410 kyr. Comparison of ^{10}Be concentrations in sediments and boulders and the ages of the fans indicate that ^{10}Be accumulation is largely controlled by the geomorphic processes that operate on the fan and not by the age of the fan.

Our data raises the intriguing issue of “the age of landscapes”. The data from fan 5, for example, shows the most extreme differences. The age of the fan is greater than 400 kyr (Matmon et al., 2005). However, the apparent ages of boulders on the fan range between 76 ka and 80 ka and the apparent age of the sediment is only ~30 ka. Our data demonstrate that surface features on a geomorphic surface may have exposure ages that do not represent the “true” landform age, thus illustrating the dynamic and ever-changing character of the landscape.

Acknowledgments

We thank Marith Rehies and Bruce Harrison for very constructive comments. We thank Y. Kolodny for great advice. We thank Ori Dor and Rachel Menashe for field assistance. This study was funded by the USGS-EHZ. This work was performed under the auspices of the U.S. Department of Energy by the University of California, Lawrence Livermore National Laboratory under Contract No. W-7405-Eng-48.

References

- Abrahams, A.D., Parsons, A.J., Cooke, R.U., Reeves, R.W., 1984. Stone movement on hillslopes in the Mojave Desert, California: a 16-year record. *Earth Surface Processes and Landforms* 9, 365–370.
- Barrows, A.G., Kahle, J.E., Beeby, D.J., 1985. Earthquake hazards and tectonic history of the San Andreas fault zone. Los Angeles County, California. California Division of Mines and Geology, Open-file report 85-10 LA, 236 p.
- Bierman, P.R., Caffee, M., 2001. Slow rates of rock surface erosion and sediment production across the Namib Desert and escarpment, Southern Africa. *American Journal of Science* 301, 326–358.
- Brown, E.T., Bourles, D.L., Burchfiel, B.C., Qidong, D., Jun, L., Molnar, P., Raisbeck, G.M., Yiou, F., 1998. Estimation of slip rates in the Southern Tien-Shan using cosmic ray exposure dates of abandoned alluvial surfaces. *Geological Society of America Bulletin* 110, 377–386.
- Clapp, E.M., Bierman, P.R., Schick, A.P., Lekach, J., Enzel, Y., Caffee, M., 2000. Sediment yield exceeds sediment production in arid region drainage basins. *Geology* 28, 995–998.
- Clapp, E.M., Bierman, P.R., Nichols, K.K., Pavich, M., Caffee, M., 2001. Rates of sediment supply to arroyos from upland erosion determined using in situ produced cosmogenic ^{10}Be and ^{26}Al . *Quaternary Research* 55, 235–245.
- Cockburn, H.A.P., Seidl, M.A., Summerfield, M.A., 1999. Quantifying denudation rates on inselbergs in the central Namib Desert using in situ-produced cosmogenic ^{10}Be and ^{26}Al . *Geology* 27, 399–402.
- Dibblee Jr., T.W., 2002a. Geologic map of the Pacifico Mountain and Palmdale Quadrangles. Dibblee Geological Foundation, map #DF-76, scale 1:24,000.
- Dibblee Jr., T.W., 2002b. Geologic map of the Juniper Hills. Dibblee Geological Foundation, map #DF-79, scale 1:24,000.
- Gilbert, G.K., 1877. *Geology of the Henry Mountains (Utah)*. U.S. Geographical and Geological Survey of the Rocky Mountain Region. Washington, DC.
- Granger, D.E., Smith, A.L., 2000. Dating buried sediments using radioactive decay and muogenic production of ^{26}Al and ^{10}Be . *Nuclear Instruments and Methods in Physics Research* 172, 822–826.
- Granger, D.E., Muzikar, P.F., 2001. Dating sediment burial with in situ-produced cosmogenic nuclides: theory, techniques, and limitations. *Earth and Planetary Science Letters* 188, 269–281.
- Granger, D.E., Kirchner, J.W., Finkel, R., 1996. Spatially averaged long-term erosion rates measured from in-situ produced cosmogenic nuclides in alluvial sediment. *Journal of Geology* 104, 249–257.
- Kirchner, J.W., Finkel, R.C., Riebe, C.S., Granger, D.E., Clayton, J.L., King, J.G., Megahan, W.F., 2001. Mountain erosion over 10 yr, 10 k.y., and 10 m.y. time scales. *Geology* 29, 591–594.
- Klein, J., Giegengack, R., Middleton, R., Sharma, P., Underwood Jr., J.R., Weeks, R.A., 1986. Revealing histories of exposure using in situ produced ^{26}Al and ^{10}Be in Libyan Glass. *Radiocarbon* 28, 547–555.
- Lal, D., 1991. Cosmic ray labeling of erosion surfaces: in situ production rates and erosion models. *Earth and Planetary Science Letters* 104, 424–439.
- Masarik, J., Wieler, R., 2003. Production rates of cosmogenic nuclides in boulders. *Earth and Planetary Science Letters* 216, 201–208.
- Matmon, A., Crouvi, O., Enzel, Y., Bierman, P., Larsen, J., Porat, N., Amit, R., Caffee, M., 2003. Complex exposure histories of chert clasts in the late Pleistocene shorelines of Lake Lisan, Southern Israel. *Earth Surface Processes and Landforms* 28, 493–506.
- Matmon, A., Schwartz, D., Finkel, R., Clemmens, S., Hanks, T., 2005. Dating offset fans along the Mojave section of the San Andreas Fault using cosmogenic ^{26}Al and ^{10}Be . *Geological Society of America Bulletin* 117, 795–807.
- McGee, W.J., 1897. Sheetflood erosion. *Bulletin of the Geological Society of America* 8, 87–112.
- Nichols, K.K., Bierman, P.R., Hooke, R.L., Clapp, E.M., Caffee, M., 2002. Quantifying sediment transport on desert piedmonts using ^{10}Be and ^{26}Al . *Geomorphology* 45, 105–125.
- Nichols, K.K., Bierman, P.R., Caffee, M.W., Finkel, R., Larsen, J., 2005. Cosmogenically enabled sediment budgeting. *Geology* 33, 133–136.
- Oberlander, T.M., 1974. Landscape inheritance and the pediment problem in the Mojave. *Geological Society of America Bulletin* 113, 241–255.
- Persico, L.P., Nichols, K.K., Bierman, P.R., 2005. Tracking painted pebbles: short-term rates of sediment movement on four Mojave Desert Piedmont Surfaces. *Water Resources Research* 41, W07004.
- Pigati, J.S., Lifton, N.A., 2004. Geomagnetic effects on time-integrated cosmogenic nuclide production with emphasis on in situ ^{14}C and ^{10}Be . *Earth and Planetary Science Letters* 226, 193–205.
- Schaller, M., von Blanckenberg, F., Hovius, N., Kubik, P.W., 2001. Large-scale erosion rates from in situ-produced cosmogenic nuclides in European river sediments. *Earth and Planetary Science Letters* 188, 441–458.
- Schick, A.P., Lekach, J., 1993. An evaluation of two ten-year sediment budgets, Nahal Yael, Israel. *Physical Geography* 14, 225–238.
- Trull, T.W., Brown, E.T., Marty, B., Raisback, G.M., Yiou, F., 1995. Cosmogenic ^{10}Be and ^3He accumulation in Pleistocene beach terraces in Death Valley, California, U.S.A.: implication for cosmic ray exposure dating of young surfaces in hot climates. *Chemical Geology* 119, 191–207.
- Wells, S.G., McFadden, L.D., Poeths, J., Olinger, C.T., 1995. Cosmogenic ^3He surface-exposure dating of stone pavements; implications for landscape evolution in deserts. *Geology* 23, 613–616.
- Zehfuss, P.H., Bierman, P.R., Gillespie, A.R., Burke, R.M., Caffee, M.W., 2001. Slip rates on the Fish Springs fault, Owens Valley, California, deduced from cosmogenic ^{10}Be and ^{26}Al and soil development on fan surfaces. *Geological Society of America Bulletin* 113, 241–255.